electronics

MDPI

Article

Capacity Optimization of Wind–Solar–Storage Multi-Power Microgrid Based on Two-Layer Model and an Improved Snake Optimization Algorithm

Mintong Zhao [1], Yuling He [2,3,4,*], Yunfeng Tian [2], Kai Sun [2], Lingyu Jiao [2] and Haipeng Wang [2,3]

[1] Power Grid Planning Research Center of Guangdong Power Grid Co., Ltd., Guangzhou 510080, China; zhaomintong@gsbb.gd.csg.cn
[2] Department of Mechanical Engineering, North China Electric Power University, Baoding 071003, China; 220232224066@ncepu.edu.cn (Y.T.); 120222102025@ncepu.edu.cn (K.S.); 220222224010@ncepu.edu.cn (L.J.); wanghpmail@ncepu.edu.cn (H.W.)
[3] Hebei Engineering Research Center for Advanced Manufacturing & Intelligent Operation and Maintenance of Electric Power Machinery, North China Electric Power University, Baoding 071003, China
[4] Suzhou Institute of North China Electric Power University, Suzhou 215000, China
* Correspondence: heyuling1@163.com

Abstract: A two-layer optimization model and an improved snake optimization algorithm (ISOA) are proposed to solve the capacity optimization problem of wind–solar–storage multi-power microgrids in the whole life cycle. In the upper optimization model, the wind–solar–storage capacity optimization model is established. It takes wind–solar power supply and storage capacity as decision variables and the construction cost of the whole life cycle as the objective function. At the lower level, the optimal scheduling model is established, considering the output characteristics of various types of power supplies and energy storage, microgrid sales, and purchases of power as constraints. At the same time, the model considers constraints, such as the power balance, the operating state of the energy storage system, the power sales and purchases, and the network fluctuations, to ensure the system operates efficiently. Taking a microgrid in South China as an application scenario, the model is solved and the optimal capacity allocation scheme of the microgrid is obtained. Meanwhile, the demand response mechanism and the influence of planning years are introduced to further optimize the configuration scheme, and the impact of different rigid–flexible load ratios and various planning horizons on microgrid capacity optimization is analyzed, respectively, by a numerical example. The comparison shows that the ISOA has better optimization performance in solving the proposed two-layer model.

Keywords: two-layer optimization model; capacity optimization; optimized scheduling; improved snake optimization algorithm; demand response; electrical power system

check for updates

Citation: Zhao, M.; He, Y.; Tian, Y.; Sun, K.; Jiao, L.; Wang, H. Capacity Optimization of Wind–Solar–Storage Multi-Power Microgrid Based on Two-Layer Model and an Improved Snake Optimization Algorithm. *Electronics* **2024**, *13*, 4315. https://doi.org/10.3390/electronics13214315

Academic Editors: Jianguo Zhu and Dorin Petreus

Received: 19 September 2024
Revised: 22 October 2024
Accepted: 31 October 2024
Published: 2 November 2024

Copyright: © 2024 by the authors. Licensee MDPI, Basel, Switzerland. This article is an open access article distributed under the terms and conditions of the Creative Commons Attribution (CC BY) license (https://creativecommons.org/licenses/by/4.0/).

1. Introduction

With the growth of energy demand and the urgent need for environmentally friendly energy, microgrid systems have attracted increasing attention as a flexible and sustainable energy solution [1]. A microgrid is a small distribution system composed of distributed power sources, load, distribution equipment, and monitoring and protection devices. Compared with the traditional power system, a microgrid features numerous distributed power sources, energy storage, and new load access. This results in new morphological characteristics in the power system, such as power supply diversification, source–load interaction, power electronic integration, and intelligent control [2]. Its capacity allocation becomes more complex, and higher requirements are demanded for economic dispatch.

A large number of scholars have conducted research on the capacity optimization and allocation of microgrids and have achieved notable research results. In [3], Fu et al.

proposed a capacity optimization design for an electrified gas storage system based on a genetic algorithm, which could better meet the needs of an independent power system and improved its reliability and stability. In [4], Modu et al. proposed a framework for efficient design and evaluation of an independent hybrid renewable energy system that met the energy needs of a rural community in Northeast Nigeria. The successful implementation of an energy management system led to the establishment of an environmentally friendly and cost-effective energy system. In [5], Yang et al. focused on a microgrid system that incorporated hybrid energy storage systems, real-time price demand response, and distribution networks. The study aimed to address the supply and demand uncertainties brought about by the high penetration rate of electric vehicles, thereby ensuring the security of the power system. In [6], Hemmati et al. focused on the energy challenges of Lombok Island, Indonesia, particularly the imbalance between peak and base load demands. The focus was on evaluating both the environmental and economic impacts of these batteries using a life cycle assessment and life cycle costing approach. In [7], Wang et al. proposed a multi-strategy snake optimizer based on opposition learning, adaptive weight factor, and Levy flight strategy. The proposed method was designed to effectively improve the accuracy and stability of the non-convex capacity optimization model for hybrid energy storage systems.

In the research of microgrid optimization scheduling, a large number of scholars also carried out corresponding work and achieved numerous practical engineering results, and promoted the transformation and development of the power system. In [8], Mu et al. used an improved deep reinforcement learning algorithm to solve the optimal scheduling problem of microgrids under uncertain conditions. In [9], Chen et al. aimed at distributed economic scheduling (DES) for the privacy protection of independent microgrids. An accelerated consensus scheme based on short-term memory was adopted to improve the convergence speed of the DES algorithm. In [10], Hemmati et al. proposed a multi-microgrid energy management method that optimized battery storage, renewable energy, and demand response. The model optimized costs through Mixed-Integer Linear Programming and evaluated power procurement and exchange in a sample network with DC power flow constraints. In [11], Hemmati et al. proposed a risk-based optimal scheduling method for a reconfigurable smart microgrid to maximize operator profit. A TVAC-PSO algorithm was applied to optimize microgrid switch configurations, with a constraint on the number of topology changes. The approach incorporated a conditional value-at-risk measure to manage risk, and the results showed improved profits and longer periods of power sales to the upstream network. In [12], Chen et al. developed a quantitative distributed optimization algorithm using the Paillier cryptograph-decryption scheme.

In recent years, a large number of scholars have applied two-layer optimization to research in power and energy systems. The two-layer optimization model has the characteristics of hierarchy, independence, conflict, priority and autonomy. The two-layer optimization model solves the disadvantages of low efficiency of the traditional single-layer optimization in solving the optimization problems of large scale and complex structure. For complex models of power grids, the two-layer optimization model can address the optimization problems efficiently and reliably. In [13], Yan et al. aimed at addressing the increasing problem of global environmental pollution and the demand for energy structure adjustment, and proposed a comprehensive energy system planning model. In [14], Hemmati et al. proposed a two-stage stochastic model aimed at minimizing total operational costs while accounting for uncertainties in wind energy, electrical load, and real-time power prices. The model addressed challenges related to the interconnection of power and gas networks. In [15], Wang et al. used a two-layer collaborative optimization approach to configure the device capacity and found the best variable operating strategy and electric cooling ratio. In [16], Ji et al. addressed the trend of large-scale participation of renewable energy in future electricity market bidding. The authors proposed a two-layer bidding strategy based on deep reinforcement learning and utilized the equilibrium supply function as the market clearing model. In [17], Phommixay et al. emphasized the

importance of microgrids in the sustainable development of cities and communities and proposed a novel two-layer model. The approach was designed to minimize the total operating costs of microgrids under high-dimensional uncertainties such as generators, load demands, and planned outages.

Although the above literature has achieved significant results, there are still many problems in the development of microgrids in the context of energy transformation. In terms of capacity optimization, most research only considers single power supplies or energy storage configurations [18,19]. However, in engineering, the power supply of microgrids is increasingly diversified, and the structure varies. Therefore, the optimal capacity of single power supplies or energy storage configurations can no longer meet the requirements of engineering applications. With the construction of smart grids being in full swing, it is becoming more and more important to optimize power grid scheduling, especially with higher requirements for algorithms to meet these needs. To meet the demands of the smart grid, more advanced and efficient algorithms are required to fulfill engineering requirements. Meanwhile, few scholars have combined the optimal allocation problem with optimal scheduling. Aiming at the medium- and long-term operation of microgrids, this paper adopts a two-layer optimal allocation method, which combines the optimal allocation problem with optimal scheduling, and proposes an ISOA to optimize the capacity of microgrids. At the same time, the influence of different rigid–flexible load ratios on the capacity of microgrids under the time-of-use (TOU) tariff mechanism is analysed, and the cost composition under different planning years is also analysed. Finally, the capacity optimization allocation scheme of the whole life cycle of a wind–solar microgrid is obtained.

2. Microgrid System Model

2.1. System Structure

A microgrid is mainly composed of wind turbines, photovoltaic arrays, energy storage devices, converters and local loads, which are connected to the upper power grid [20]. This paper studies a small microgrid. To meet the needs of the microgrid, surplus power is sold to the main power grid to enhance the system's economic efficiency. In addition, when there is a power shortage in the system, power is purchased from the upper power grid to ensure the reliability of the system. The system structure is shown in Figure 1.

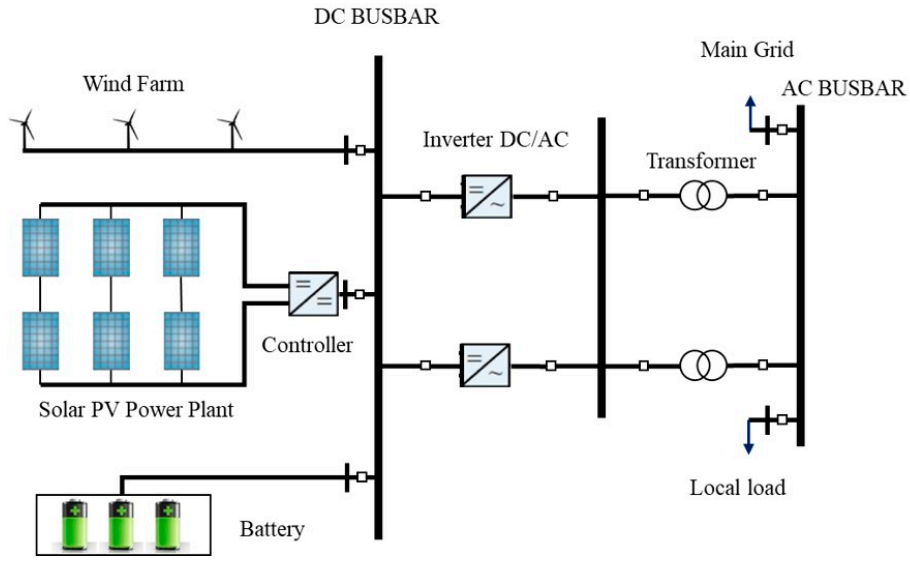


Figure 1. Microgrid system structure.

2.2. Power Supply Model

The output characteristics of wind turbines are related to a variety of environmental factors, mainly determined by wind speed, which can be approximated as a piecewise function [21].

$$P_{WT} = \begin{cases} 0 & 0 \le v \le v_{ci} \\ P_r \frac{v - v_{ci}}{v_r - v_{ci}} & v_{ci} < v \le v_r \\ P_r & v_r < v \le v_{co} \\ 0 & v > v_{co} \end{cases} \quad (1)$$

where P_{WT} indicates the output power of a wind turbine. P_r indicates the rated power of the wind turbine. v indicates the real-time wind speed. v_{ci} indicates the cut-in wind speed. v_{co} indicates cut-out wind speed. v_r indicates the rated wind speed.

The output power of photovoltaic modules is related to factors such as solar radiation, ambient temperature and rated power under standard conditions, and its output model [22] can be expressed as

$$P_{PV}(t) = P_{STC} \frac{G_c(t)}{G_{STC}} \{1 + k[T_c(t) - T_{STC}]\} \quad (2)$$

where $P_{PV}(t)$ indicates the output power of a photovoltaic array at time t. P_{STC} indicates the rated output power of a photovoltaic array under standard conditions. G_{STC} indicates the illumination intensity under standard conditions. $G_c(t)$ indicates the actual illumination intensity at the working point. k indicates the power temperature coefficient. $T_c(t)$ indicates the operating temperature at time t. T_{STC} indicates the operating temperature under standard conditions.

2.3. Battery Model

In a grid-connected microgrid, the battery enhances the system's energy utilization, reduces dependence on the main power grid, and improves overall system economy. Additionally, it helps mitigate grid fluctuations and enhances power quality. When the system is in a defect state, it discharges; otherwise, it charges. The output model [23] is as follows:

System discharge:

$$SOC(t) = SOC(t-1)(1-\sigma) + \frac{P_c(t)\Delta t \eta_c}{E_b} \quad (3)$$

System charge:

$$SOC(t) = SOC(t-1)(1-\sigma) - \frac{P_d(t)\Delta t}{E_b \eta_d} \quad (4)$$

where $SOC(t)$ indicates the remaining power of the battery at time t. s indicates the self-discharge rate of the battery per hour. Δt is the time step. P_c and P_d indicate the charging and discharging power of the battery in the t time period, respectively. h_c and h_d indicate the charging and discharging efficiency of the battery, respectively. E_b indicates the rated capacity of the battery.

2.4. Demand Response Under the TOU Tariff Mechanism

Demand response refers to the mechanism by which users change their electricity consumption behavior by responding to price signals or incentive signals [24]. According to the response mode, demand response can be categorized into price-based demand response and incentive-based demand response. Among them, the price-based demand response has the advantages of a large adjustment range, wide range, long implementation time and stability, which can effectively change the user's behavior of electricity consumption, and has a positive role in promoting the full absorption of wind power generator and photovoltaic power.

The load can usually be simply divided into the following two categories:

Rigid load: Rigid load refers to the load with relatively high priority, which has a greater impact on production and life and does not participate in the response. Flexible load: The power consumption time of flexible load can be interrupted, not constrained by continuity, and can be transferred from one time period to another time period, but the total power consumption within the entire scheduling cycle must be ensured.

As a commodity, electric energy shares common characteristics with other goods, and its price is generally inversely proportional to demand, as illustrated in Figure 2.

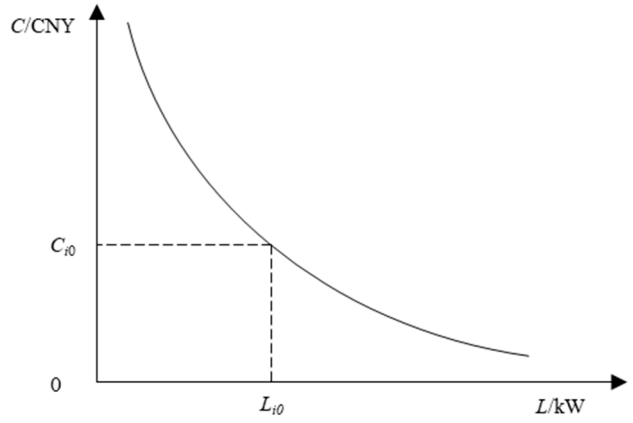


Figure 2. Demand curve.

The customer's response to electricity price is often described by the demand elasticity coefficient.

$$\begin{cases} \varepsilon_{mn} = \frac{\Delta L_i(m) C_{i0}(n)}{L_{i0}(m) \Delta C_i(n)} \\ \Delta L_i(m) = L_i(m) - L_{i0}(m) \\ \Delta C_i(n) = C_i(n) - C_{i0}(n) \end{cases} \tag{5}$$

where ε_{mn} indicates the demand elasticity coefficient of user i. When the time m equals n, it represents the self-elasticity coefficient, and its value is negative. As electricity prices rise, user demand decreases accordingly. When the time m does not equal n, it represents the self-elasticity coefficient, and its value is positive. When the electricity price at time n decreases, users shift part of their load from time m to time n; conversely, if the price increases at time n, users shift their load from time n to time m. $\Delta L(m)$ indicates the change in electricity at time m. $\Delta C(n)$ indicates the change in electricity price at time n. $L_{i0}(m)$ indicates the amount of electricity at time m before the TOU tariff is applied. $C_{i0}(n)$ indicates the price of electricity at time n before the TOU tariff is applied. $L_i(m)$ indicates the electricity quantity at time n after the TOU tariff is applied. $C_i(n)$ indicates the price of electricity at time n after the TOU tariff is applied.

$$E = \begin{bmatrix} \varepsilon_{11} & \varepsilon_{12} & \cdots & \varepsilon_{1t} \\ \varepsilon_{21} & \varepsilon_{22} & \cdots & \varepsilon_{2t} \\ \vdots & \vdots & \vdots & \vdots \\ \varepsilon_{t1} & \varepsilon_{t2} & \cdots & \varepsilon_{tt} \end{bmatrix} \tag{6}$$

where t indicates the number of periods. The elastic matrix is obtained by statistical analysis of the user behavior under the historical TOU tariff mechanism.

When the demand elasticity coefficient matrix is known, the electricity quantity of each period after the implementation of TOU tariff is as follows:

$$\begin{bmatrix} L_i(1) \\ L_i(2) \\ \vdots \\ L_i(t) \end{bmatrix} = \begin{bmatrix} L_{i0}(1) \\ L_{i0}(2) \\ \vdots \\ L_{i0}(t) \end{bmatrix} + \begin{bmatrix} L_{i0}(1) & 0 & \cdots & 0 \\ 0 & L_{i0}(2) & \cdots & \vdots \\ \vdots & \vdots & \vdots & 0 \\ 0 & \cdots & 0 & L_{i0}(t) \end{bmatrix} E \begin{bmatrix} \frac{\Delta C_i(1)}{C_{i0}(1)} \\ \frac{\Delta C_i(2)}{C_{i0}(2)} \\ \vdots \\ \frac{\Delta C_i(t)}{C_{i0}(t)} \end{bmatrix} \quad (7)$$

3. Capacity Optimization Allocation Based on Two-Layer Optimization Model

The capacity optimization method utilizes a two-layer optimization model, in which the upper-layer model is the capacity optimization model and the lower-layer model is the optimal scheduling model. The capacity optimization model uses wind speed, illumination intensity, and load data as inputs. With the installed capacity of wind turbines, photovoltaic arrays and batteries as the decision variables, and the minimum comprehensive cost as the objective function, the capacity allocation scheme is calculated as the input of the optimal scheduling model. The flow chart of the two-layer optimization model used in this paper and the relationship between the upper and lower models are shown in Figure 3.

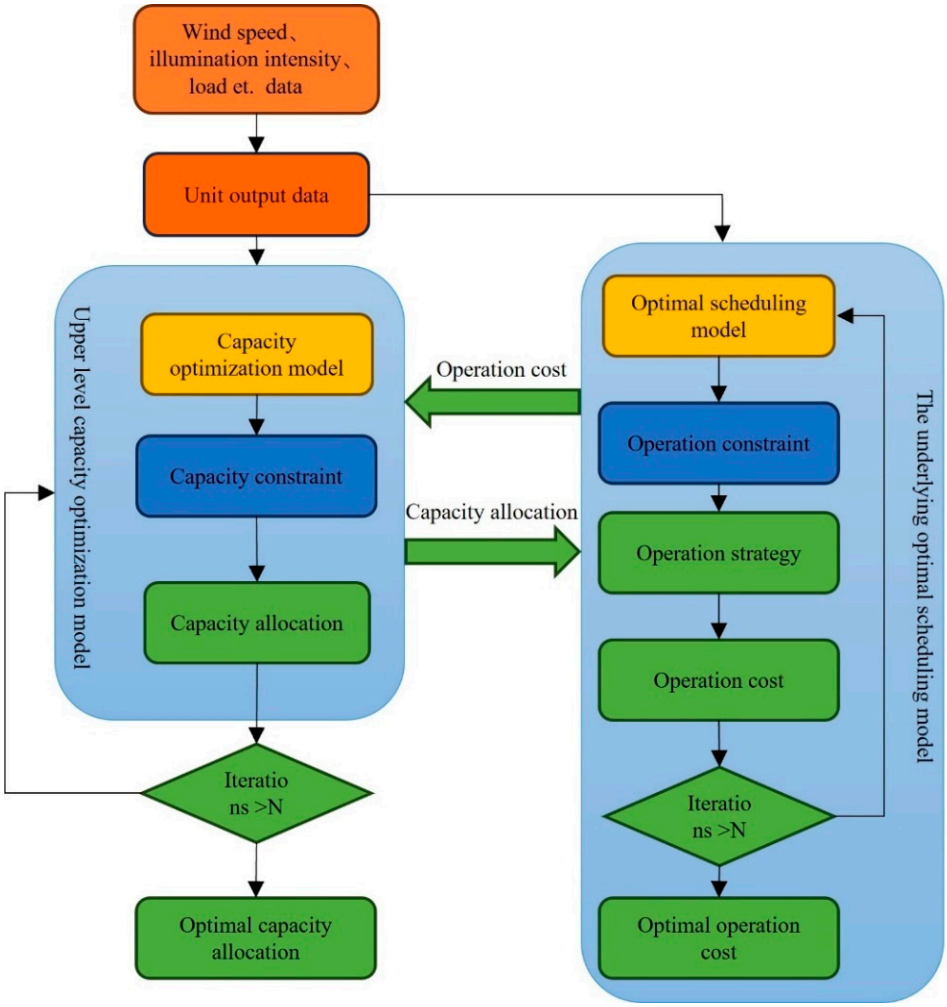


Figure 3. Flow chart of two-layer optimization configuration.

3.1. Capacity Optimization Model

3.1.1. Objective Function of Capacity Optimization Model

Capacity optimization of the microgrid aims to determine the installed capacity of wind turbines, photovoltaic arrays and batteries according to the load demand in a microgrid. The decision variables of the optimization model can be expressed as

$$x = [N_{wind}, N_{pv}, N_{batt}] \tag{8}$$

where N_{wind} indicates the installed number of wind turbines. N_{pv} indicates the installed number of photovoltaic arrays. N_{batt} indicates the installed number of batteries.

Capacity optimization aims for the lowest comprehensive cost, including construction cost, periodic replacement costs of components, and operating cost.

$$\min C = C_{wind} + C_{pv} + C_{batt} + C_{oper} \tag{9}$$

where C_{wind}, C_{pv}, and C_{batt} represent the present value of the construction and periodic replacement costs for wind turbines, photovoltaic arrays, and batteries in a wind–solar–storage power generation system, respectively. C_{oper} indicates the operating cost of the microgrid during the planned life, which is obtained by the scheduling model of the lower-level model.

The specific expression of the cost of microgrid construction and periodic replacement of components is as follows:

$$\begin{cases} C_{wind} = C_{1,wind}N_{wind} + \frac{C_{2,wind}N_{wind}}{(1+r)^{T_{wind}}} \\ C_{pv} = C_{1,pv}N_{pv} + \frac{C_{2,pv}N_{pv}}{(1+r)^{T_{pv}}} \\ C_{batt} = C_{1,batt}N_{batt} + \frac{C_{2,batt}N_{batt}}{(1+r)^{T_{batt}}} \end{cases} \tag{10}$$

where $C_{1,wind}$, $C_{1,pv}$ and $C_{1,batt}$ indicate the unit construction costs of wind turbines, photovoltaic arrays, and batteries, respectively. $C_{2,wind}$, $C_{2,pv}$ and $C_{2,batt}$ indicate the unit replacement costs of wind turbines, photovoltaic arrays, and batteries, respectively. T_{wind}, T_{pv}, and T_{batt} indicate, respectively, the life cycles of wind turbines, photovoltaic arrays, and batteries. r indicates the discount rate.

3.1.2. Constraint Condition of Capacity Optimization Model

Due to the influence of site, environment, and other factors, the capacity allocation needs to be constrained by the capacity size.

$$\begin{cases} P_{wind,\min} \le N_{wind}P_{wind,unit} \le P_{wind,\max} \\ P_{pv,\min} \le N_{pv}P_{pv,unit} \le P_{pv,\max} \\ E_{batt,\min} \le N_{batt}E_{batt,unit} \le E_{batt,\max} \end{cases} \tag{11}$$

where $P_{wind,unit}$, $P_{pv,unit}$ and $E_{batt,unit}$ indicate, respectively, the capacity of wind turbines, photovoltaic arrays and batteries. $P_{wind,min}$, $P_{pv,min}$ and $E_{batt,min}$ indicate, respectively, the lower limits of the installed capacity of wind turbines, photovoltaic arrays and batteries. $P_{wind,max}$, $P_{pv,max}$ and $E_{batt,max}$ indicate, respectively, the upper limits of the installed capacity of wind turbines, photovoltaic arrays and batteries.

3.2. Optimized Scheduling Model

3.2.1. Objective Function of Optimized Scheduling Model

The optimal scheduling model takes the system operation cost as the objective function, and the specific expression is as follows:

$$\min C_{oper} = \sum_{k=1}^{T_z} \left(C_{oper,wind} + C_{oper,pv} + C_{oper,batt} + C_{grid} \right) \tag{12}$$

where $C_{oper,wind}$, $C_{oper,pv}$ and $C_{oper,batt}$ indicate, respectively, the annual operation costs of wind turbines, photovoltaic arrays and batteries. C_{grid} indicates the power purchase cost of the interaction between the microgrid and the main grid. T_z indicates the planned period.

The specific expression of the annual operation cost of wind turbines, photovoltaic arrays and batteries is as follows:

$$\begin{cases} C_{oper,wind} = \sum_{t=1}^{8760} \alpha_{wind} P_{WT} N_{wind} \Delta t \\ C_{oper,pv} = \sum_{t=1}^{8760} \alpha_{pv} P_{PV} N_{pv} \Delta t \\ C_{oper,batt} = \sum_{t=1}^{8760} \alpha_{batt} a_t P_{batt} \Delta t \end{cases} \tag{13}$$

where α_{wind} and α_{pv} indicate the operation costs per unit of power generation of wind turbines and photovoltaic arrays, respectively. α_{batt} indicates the operation cost per unit discharge of the battery. a_t (a_t = {0,1}) indicates the charge and discharge identifier of the battery. a_t = 0 when the battery is charged, and a_t = 1 when the battery is discharged. P_{batt} indicates the charging and discharging power of a battery.

The specific expression of the power purchase cost of the interaction between the microgrid and main grid is as follows:

$$\begin{cases} C_{grid} = C_{buy} - C_{sell} \\ C_{buy} = \sum_{t=1}^{8760} b_t \sigma_1 (P_{load} - P_{WT} - P_{PV} - P_{batt}) \Delta t \\ C_{sell} = \sum_{t=1}^{8760} c_t \sigma_2 (P_{WT} + P_{PV} + P_{batt} - P_{load}) \Delta t \end{cases} \tag{14}$$

where C_{buy} indicates the cost of purchasing power from the microgrid to the main grid. C_{sell} indicates the income from the sale of electricity from the microgrid to the main grid. P_{load} indicates the load power. b_t (b_t = {0,1}) is the power purchase identifier. When the power supply in the microgrid is greater than the load, b_t = 1; otherwise, b_t = 0. c_t (c_t = {0,1}) is the electricity sale identifier. When the power supply in the microgrid is less than the load, c_t = 1; otherwise, c_t = 0. σ_1 and σ_2 indicate, respectively, the electricity purchase price and the electricity sale price.

3.2.2. Constraint Condition of Optimized Scheduling Model

(1) The power balance constraint is as follows:

$$P_{WT} + P_{PV} + P_{batt} + P_{grid} = P_{load} \tag{15}$$

where P_{gird} indicates the power exchange between the microgrid and the main grid. P_{batt} and P_{grid} can be either positive or negative values.

(2) Battery constraint [25]: Battery operation constraints include the charge state, charge and discharge power constraint, charge and discharge time constraint, and start and end state constraint.

$$SOC_{\min} \leq SOC_t \leq SOC_{\max} \tag{16}$$

where SOC_t indicates the charged state of the battery at time t. $SOC_{\min}$ and $SOC_{\max}$ indicate the maximum and minimum values of the charged state of the battery, respectively. Generally, the minimum charged state $SOC_{\min}$ = 0~0.2, and the maximum charged state $SOC_{\max}$ = 0.8~0.9. In this paper, the minimum value of charged state $SOC_{\min}$ = 0.2, and the maximum value of charged state $SOC_{\max}$ = 0.8.

In the unit time, the charge state of the battery caused by the charge and discharge of the battery is uniform and can be expressed as

$$\begin{cases} SOC_t = SOC_{t-1}(1-\delta) + \eta_c \frac{P_{cha,t}\Delta t}{E_{batt}} \mathrm{X}_t \\ SOC_t = SOC_{t-1}(1-\delta) - \eta_d \frac{P_{dis,t}\Delta t}{E_{batt}} \Upsilon_t \end{cases} \tag{17}$$

where δ indicates the self-discharge rate. The value is 0.001. η_c and η_d indicate the charging and discharging efficiency of the battery, respectively. $P_{cha,t}$ and $P_{dis,t}$ indicate the charging and discharging power of the battery at time t, respectively. X_t and Υ_t are charge and discharge labels of batteries; that is, X_t = {0,1} and Υ_t = {0,1}. When X_t = 1 and Υ_t = 0, the battery is charged. On the other hand, when X_t = 0 and Υ_t = 1, the battery is discharged. E_{batt} indicates the rated capacity of the battery.

To protect the battery and prolong its service life, the battery must be in the charged state within adjacent periods.

$$|SOC_t - SOC_{t-1}| \leq 0.2 \tag{18}$$

In order to improve reliability and safety, the battery can not discharge while charging. At the same time, the charge and discharge capacity of the battery should not exceed 20% of the capacity in one hour, as shown below:

$$\begin{cases} \mathrm{X}_t \cdot \Upsilon_t = 0 \\ 0 \leq P_{cha,t}\Delta t \leq 0.2 E_{batt} \mathrm{X}_t \\ 0 \leq P_{dis,t}\Delta t \leq 0.2 E_{batt} \Upsilon_t \end{cases} \tag{19}$$

The charge and discharge frequency of a battery is closely related to its service life. Therefore, the number of charges and discharges of a battery should be constrained.

$$\begin{cases} \sum |\mathrm{X}_{t+1} - \mathrm{X}_t| \leq N_1 \\ \sum |\Upsilon_{t+1} - \Upsilon_t| \leq N_2 \end{cases} \tag{20}$$

where N_1 is the maximum charge number. N_2 is the maximum discharge number.

In addition, the initial state, SOC_0, should be the same as the end state, SOC_T, in a scheduling period.

$$SOC_0 = SOC_T \tag{21}$$

(3) Main grid access power fluctuation constraints: The energy storage device must smooth the power fluctuation caused by the wind–photovoltaic power generation into the grid to meet the grid standard and load demand. Therefore, the power fluctuation of the microgrid should be satisfied after the energy storage device is added.

$$\begin{cases} D_{grid} = \frac{P_{grid,\max} - P_{grid,\min}}{\Delta t'} \\ D_{grid} \leq \varepsilon_{grid} \end{cases} \tag{22}$$

where D_{grid} indicates the power exchange rate between the microgrid and the main grid. $P_{grid,\max}$ and $P_{grid,\min}$ are, respectively, the maximum and minimum values of power exchange between the microgrid and the main grid. Dt' indicates the time interval between the maximum and minimum values. ε_{grid} indicates the power fluctuation standard.

4. Model Solving Method Based on Improved Snake Optimization Algorithm

The snake optimization algorithm (SOA) is an optimization algorithm proposed by Hashim et al. [26]. The algorithm divides snake groups into male and female groups with the same number of individuals. Assuming the total number of snake groups is Np, the number of male and female snake groups is $N_m = N_f = N_{p/2}$, respectively. The algorithm is divided into global exploration and local development stages. SOA is a relatively effective

optimization algorithm. However, it often falls into local optima, indicating insufficient global search capability. Therefore, in order to enhance the search ability of SOA for global optimization and speed up the convergence of the algorithm, the following ISOA is proposed.

4.1. Improved Snake Optimization Algorithm

4.1.1. Snake Colony Position Initialization Based on Tent Chaotic Mapping and Quasi-Reverse Learning Strategy

The diversity of the initial position of the population is crucial for achieving the global optimal solution in the snake optimization algorithm. Chaotic mapping is characterized by strong randomness, ergodicity, regularity and sensitivity to initial values, which can help the algorithm jump out of the local optimal solution and obtain better global optimal search ability. Additionally, the Tent chaotic map generates random numbers uniformly in the range of [0,1], which can make the location of the initial population generated by the algorithm more diverse [27]. Therefore, this paper introduces Tent chaotic mapping to initialize the position of the snake colony.

The chaotic sequence based on Tent chaotic mapping is as follows:

$$z_{i+1} = \begin{cases} \frac{z_i}{\varepsilon}, & 0 \le z_i \le \varepsilon \\ \frac{1-z_i}{1-\varepsilon}, & \varepsilon < z_i \le 1 \end{cases} (i = 1, 2, \cdots) \tag{23}$$

where z_i is the i th chaotic value of the chaotic sequence. ε is the control parameter, $\varepsilon \in [0,1]$, and the value in this paper is 0.6 [28].

According to Equation (23), it can be obtained that the initial position of the snake group individual based on Tent chaotic mapping is as follows:

$$X_i = b_0 + z_i(b_1 - b_0) \quad (i = 1, 2, \cdots, N_p) \tag{24}$$

where b_1 and b_0 indicate the upper and lower bounds of the solution space, respectively. In order to further improve the diversity of the initial position of the snake group, a quasi-reverse learning strategy was introduced. Based on the basic principle of quasi-reverse learning, there is a point x ($x \in [c_1, c_2]$) where c_1 and c_2 are the minimum and maximum values of the value interval of x, respectively. And its quasi-reverse point x^* is defined as

$$x^* = \frac{c_1 + c_2}{2} + (\frac{c_1 + c_2}{2} - x)r_d \tag{25}$$

According to Equation (25), x^* is a uniformly distributed random number in the interval $[(c_1 + c_2)/2, c_1 + c_2 - x]$. Tent chaotic mapping and quasi-reverse learning strategy are combined to form a Tent chaotic map–quasi-reverse learning strategy. According to Equations (24) and (25), it can be obtained that the initial position of the individual in the snake group based on the strategy of Tent chaotic map–quasi-reverse learning is as follows:

$$P_i = \begin{cases} \frac{b_0+b_1}{2} + (\frac{b_0+b_1}{2} - X_i)r_d & r_d \le p_r \\ X_i & else \end{cases} \tag{26}$$

where P_i indicates the initial position of the I-th snake; p_r indicates the quasi-reverse learning probability of the snake group; and p_r = 0.3 in this paper.

During the initialization of the snake colony position, the initial position X of the snake colony based on Tent chaotic mapping is mixed with the initial position P of the snake colony generated by the Tent Chaotic map–quasi-reverse learning strategy to form a mixed initial position $X_c = \{X \cup P\}$. According to the fitness size, the positions with N_p fitness value in X_c were selected as the initial locations of the snake group.

4.1.2. Snake Population Position and Fitness Update Based on Snake Optimization Algorithm

Suppose that the solution space is the foraging space of the snake group, and define the amount of food in the space as

$$Q = 0.5e^{\left(\frac{t_c}{N_{\max}} - 1\right)} \tag{27}$$

where t_c indicates the number of iterations. $N_{\max}$ is the maximum number of iterations.

When the food quantity is lower than the threshold value $T_{h1} = 0.25$, that is, when $Q < 0.25$, the snake group enters the global exploration stage, and the position update can be expressed as

$$\begin{cases} X_{i,m}(t+1) = X_{r,m}(t) \pm 0.05e^{-\frac{f_{r,m}}{f_{i,m}}}((b_1 - b_0)r_d + b_0) \\ X_{i,f}(t+1) = X_{r,f}(t) \pm 0.05e^{-\frac{f_{r,f}}{f_{i,f}}}((b_1 - b_0)r_d + b_0) \end{cases} (i, r = 1, 2, \cdots, N_p) \tag{28}$$

where $X_{i,m}$ and $X_{i,f}$ indicate the positions of the i th male and female snakes, respectively. $X_{r,m}$ and $X_{r,f}$ indicate random individual positions in male and female snake groups, respectively. $f_{r,m}$ and $f_{r,f}$ are $X_{r,m}$ and X_r respectively, and f corresponds to fitness. $f_{i,m}$ and $f_{i,m}$ are the fitness of the i th male and female snakes, respectively. r_d is random in the range of (0,1). When the amount of food is above the threshold T_{h1}, i.e., $Q > 0.25$, the snake population enters the local development stage. At this stage, the snake population is mainly affected by the ambient temperature. Define the ambient temperature as

$$T = e^{\frac{-t_c}{N_{\max}}} \tag{29}$$

In the local development stage, when the ambient temperature is higher than the threshold $T_{h2} = 0.6$, that is, $Q > 0.25$ and $T > 0.6$, the snakes only eat the stored food in the habitat, and the position update of the male and female individuals is expressed as

$$\begin{cases} X_{i,m}(t+1) = X_{fd}(t) \pm 2T(X_{fd} - X_{i,m}(t))r_d \\ X_{i,f}(t+1) = X_{fd}(t) \pm 2T(X_{fd} - X_{i,f}(t))r_d \end{cases} (i = 1, 2, \cdots, N_p/2) \tag{30}$$

where X_{fd} indicates the food location of the snake group, that is, the global optimal.

Otherwise, the snakes will engage in courtship behavior, during which the snakes choose to mate with the opposite sex or attack the same sex according to the random probability P_r ($P_r \in (0,1)$).

When $P_r > 0.6$, the snakes engage in heterosexual mating behavior, and the position update of the male and female individuals is expressed as

$$\begin{cases} X_{i,m}(t+1) = X_{i,m}(t) + 2e^{\frac{-f_{i,f}}{f_{i,m}}}(QX_{i,f}(t) - X_{i,m}(t))r_d \\ X_{i,f}(t+1) = X_{i,f}(t) + 2e^{\frac{-f_{i,m}}{f_{i,f}}}(QX_{i,m}(t) - X_{i,f}(t))r_d \end{cases} (i = 1, 2, \cdots, N_p/2) \tag{31}$$

When $P_r < 0.6$, the snakes stop the heterosexual mating behavior and turn to homosexual aggression, and the position update of the male and female individuals is expressed as

$$\begin{cases} X_{i,m}(t+1) = X_{i,m}(t) + 2e^{\frac{-f_{b,r}}{f_{i,m}}}(QX_{b,f}(t) - X_{i,m}(t))r_d \\ X_{i,f}(t+1) = X_{i,f}(t) + 2e^{\frac{-f_{b,m}}{f_{i,r}}}(QX_{b,m}(t) - X_{i,f}(t))r_a \end{cases} (i = 1, 2, \cdots, N_p/2) \tag{32}$$

where $f_{b,m}$ and $f_{b,f}$ indicate the optimal fitness values of male and female snake groups, respectively. $X_{b,m}$ and $X_{b,f}$ indicate the optimal current positions of male and female snake groups, respectively.

4.1.3. Snake Colony Position and Fitness Update of Cuckoo Search Algorithm Based on Cauchy Variation

The cuckoo search algorithm (CSA) was proposed by Yang et al. [29]. The inspiration of the algorithm came from the behavior of cuckoo birds searching for nests to hatch eggs. The algorithm adopts Levy flight strategy, which has a strong ability to jump out of local optima. The heavy-tailed characteristics of the Levy distribution make it suitable for capturing the occasional large deviations in power output, which helps improve the robustness of the optimization model in handling these uncertainties. Therefore, this paper introduces CSA into SOA to enhance the ability of the algorithm to jump out of local optima and global search.

Based on the cuckoo nest search strategy, if the number of individuals in the flock is n, when the birds search for a new nest, the position update of the cuckoo birds is expressed as

$$D_i(t+1) = D_i(t) + \alpha(D_i(t) - D_b)L \quad (i = 1, 2, \cdots, n) \tag{33}$$

where α indicates the step control factor of cuckoo flight, $\alpha \in (0,1)$; D_b is the optimal position of cuckoo birds. L is a random search path subject to Levy distribution, and the calculation formula is expressed as

$$L = \frac{u}{|v|^{1/1.5}} \tag{34}$$

where both u and v are normal distribution functions, obeying $N(0,0.6966)$ and $N(0,1)$, respectively. Cuckoos incubate their eggs in their own nests but also borrow other nests to incubate their eggs, and the probability of being found by the host is 0.25. At this point, the position update of the individual in the cuckoo flock is expressed as

$$D_i(t+1) = \begin{cases} D_i(t) + (D_p(t) - D_p(t))r_d & r_d > 0.25 \\ D_i(t+1) & r_d \leq 0.25 \end{cases} (i = 1, 2, \cdots, n) \tag{35}$$

where $D_p(t)$ and $D_q(t)$ represent the positions of any two birds in the cuckoo flock other than individual i at the t iteration. In CSA, step control factor α is used to control the search area of the algorithm. A larger value of α is conducive to global search, while a smaller value is conducive to local development. In practical application, $\alpha = 1$ is usually taken, which makes it difficult to balance the global exploration ability and local development ability in calculation. Based on this, Cauchy variation optimization is introduced to make each cuckoo obtain different flight step control factors, so as to promote the global optimization search ability of the algorithm.

The Cauchy variation is derived from the Cauchy distribution, whose cumulative distribution function is expressed as

$$F(\xi) = \frac{1}{2} + \frac{1}{\pi}\arctan(10\xi - 10\mu) \tag{36}$$

where ξ indicates the random variable of the Cauchy distribution. μ indicates a positional parameter.

For Equation (36), if $F(\xi)$ = rd, the variable ξ is expressed as

$$\xi = \mu - \frac{1}{10\tan(\pi r_d)} \tag{37}$$

In order to improve the adaptability of the cuckoo search algorithm, random variable ξ in Cauchy distribution is used as step control factor α. Therefore, the flight step control factor of any cuckoo can be expressed as

$$\alpha_i = \mu_i - \frac{1}{10\tan(\pi r_d)} \quad (1 = 1, 2, \cdots, n) \tag{38}$$

where μ_i indicates the position parameter of the i th cuckoo, and its calculation formula is expressed as

$$\mu_i = 0.1\mu_{i-1} + 0.9L_s \quad (i = 1, 2, \cdots, n) \tag{39}$$

where L_s indicates the Lehmer average, which is used to balance the trade-off between extreme values and the overall average in the system's performance metrics. The calculation method is shown in reference [30]. Equation (39) is a recursive expression, and the initial value of positional parameter μ_i is $\mu_0 = 0.5$.

Equations (33)~(35), (37) and (39) can implement the Cauchy variation cuckoo search algorithm (CVCSA) improvement of the standard SOA. When the search strategy is for cuckoo birds to find their own nest or incubate their eggs in another nest undetected by the host, the position update of the male individual in the snake colony is expressed as

$$X_{i,m}(t+1) = X_{i,m}(t) + \alpha_{i,m}(X_{i,m}(t) - X_{b,m})L_{i,m} \tag{40}$$

where $\alpha_{i,m}$ indicates the control factor for the flight step length of Cauchy-variant cuckoo in male snakes. $L_{i,m}$ represents the Levy random search path of male individuals in the snake group.

Otherwise, the male's position update is expressed as

$$X_{i,m}(t+1) = X_{i,m}(t) + (X_{p,m}(t) - X_{q,m}(t))r_d \tag{41}$$

where $X_{p,m}$ and $X_{q,m}$ indicate the positions of any two snakes outside individual i in the male pack when the Cauchy mutant cuckoo searches.

The position renewal mode of the female individual in the snake group is the same as that of the male individual, so this article will not go into detail on this.

4.2. Solving Method

This paper addresses the upper-layer capacity optimization by using the capacities of wind turbines, photovoltaic arrays, and batteries as decision variables and optimizing their respective capacities. The lower-layer optimal scheduling uses the battery state at 24 periods per day as the decision variable and optimizes the battery state for each period. This paper demonstrates the specific solution process for the upper-layer capacity optimization. Since the lower-layer optimization scheduling is similar to the upper-layer capacity optimization, it will not be detailed here. Figure 4 illustrates the algorithm flow chart.

In ISOA, each individual in the population represents the capacity of wind turbines, photovoltaic arrays and batteries. The fitness of an individual's position indicates the economic efficiency of microgrid capacity optimization. The optimal allocation scheme of microgrid capacity can be obtained by finding the best individual positions.

The procedure for applying the algorithm is as follows.

Step 1: Initialization: Determine the objective function $f(x)$. Based on Tent chaotic mapping and the quasi-oppositional learning strategy, the snake population's positions are initialized by randomly generating n individual snakes and their positions X_i. Meanwhile, randomly divide them into female and male subpopulations. Set algorithm parameters: number of population individuals n, dimension n_d, maximum number of iterations N and other parameters. Define food quantity thresholds and ambient temperature thresholds.

Step 2: The positions of female/male individuals were updated according to Equations (28) and (30)~(32), and the fitness was calculated. Compared with the previous generation of snakes, individuals with higher fitness were retained.

Step 3: Calculate the population optima and fitness values based on the snake population obtained in Step 2, and save them as SOA-based population optima and fitness values. At the same time, the position of female/male individuals was updated according to Equations (40) and (41) of the snake group; compared with the snake group of the previous generation, the numbers of individuals should be moderately higher.

Step 4: The population optima and fitness values were calculated according to the snake group obtained in Step 3 and saved as the population optima and fitness values based on CVCSA.

Step 5: Based on SOA and CVCSA, the obtained population optimum and fitness values were compared to select the snake population optimum and fitness values.

Step 6: Determine whether the number of iterations is reached. If the number of iterations is not reached, return to Step 2. If the number of iterations is reached, the optimal solution is output.

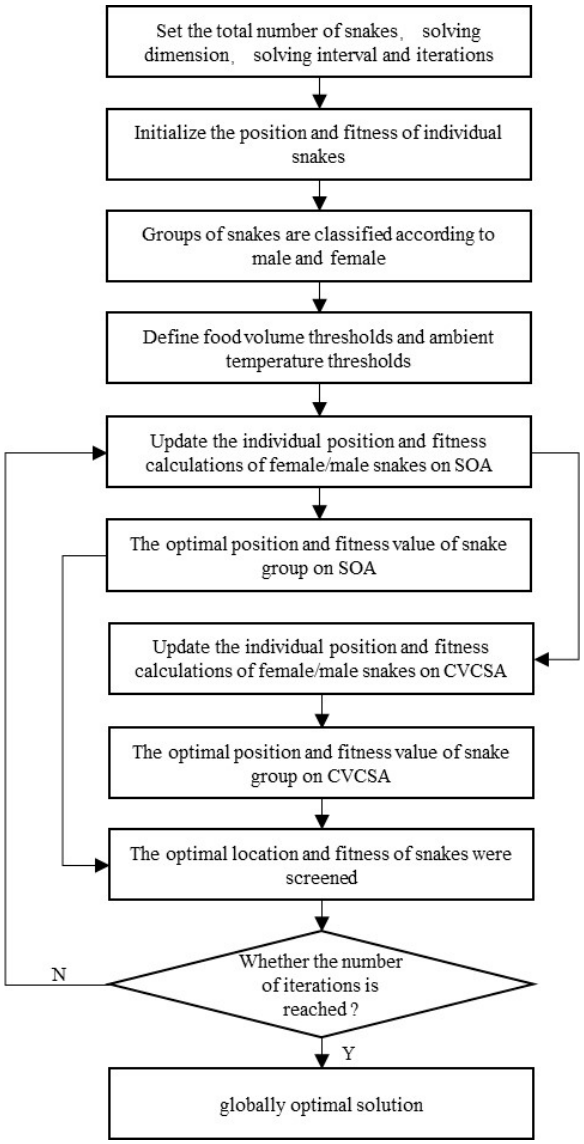


Figure 4. Calculation flow chart of ISOA.

5. Simulation Studies

5.1. Simulation Setting

In this paper, a small microgrid in southern China is taken as the background, and an example analysis is carried out based on the meteorological data of this area. The scheduling period of one day in this region is analyzed and solved. The annual wind speed and illumination intensity are shown in Figures 5 and 6, respectively. The typical daily load of the microgrid is shown in Figure 7.

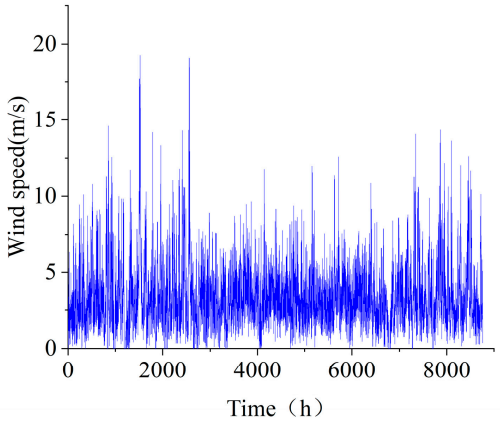


Figure 5. Annual wind velocity curve.

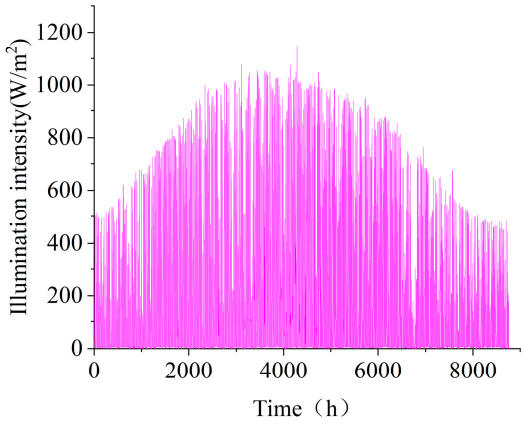


Figure 6. Annual illumination intensity curve.

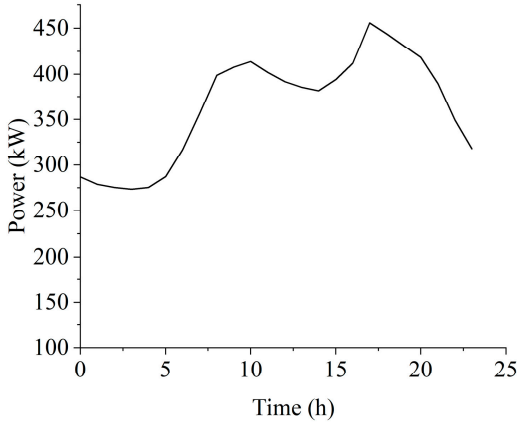


Figure 7. Typical daily load.

The rated power of the wind turbine set in this paper is 10 kW. The rated power of the unit photovoltaic array is 250 W. The rated capacity of a group of batteries is 6 kW·h. The rated power is 1.2 kW. The maximum depth of impulse discharge is 80%. The design planning lifetimes for the microgrid are 5, 10 and 20 years. The life cycle of the wind turbine and photovoltaic array exceeds the planning life, so the life cycle of the wind turbine and photovoltaic array is considered based on the design planning life. The battery life cycle is 5 years. The configuration cost of each power supply of the microgrid is shown in Table 1.

Table 1. Cost data for microgrid power supplies.

Type of Power Supply	Construction Cost (CNY/Unit)	Part Cycle Replacement Cost (CNY/kW·Year)	Operation Cost (CNY/kW·h)
Wind turbine	42,900	390	0.35
Photovoltaic array	770	7	0.58
Battery	12,000	240	0.2

The electricity price of each period is shown in Table 2, and the demand elasticity coefficient of the load is shown in Table 3. In a scheduling cycle, the state of charge of the zero-time energy storage system is 0.4, and the number of charges and discharges is less than or equal to 8 times.

Table 2. TOU price.

Period of Time	Electricity Sell Price (CNY/kW·h)	Electricity Purchase Price (CNY/kW·h)
0:00–7:00	0.22	0.25
7:00–10:00 14:00–17:00 21:00–24:00	0.42	0.53
10:00–14:00 17:00–21:00	0.65	0.82

Table 3. Demand elasticity coefficient.

Period of Time	Valley Period	Normal Period	Peak Period
Valley period	−0.100	0.010	0.012
Normal period	0.010	−0.100	0.016
Peak period	0.012	0.016	−0.100

5.2. Analysis of Optimal Allocation Results

Figure 8a represents the cost composition of the allocation stage and the operation stage. The allocation stage accounts for 19.2% of the total cost. The operation stage accounts for 80.8%. Figure 8b represents the cost composition of various types of power supplies in the allocation stage. Wind turbines account for 62.8% of the allocation cost. Photovoltaic arrays account for 11.6%. Batteries account for 25.6%. Figure 8c shows the proportion of the operating costs of various types of power supplies. Wind turbines account for 67.9% of the operating costs. Photovoltaic arrays account for 29.5%. Batteries account for 2.6%. The scheduling situation of a typical day of the two-layer optimization model is shown in Figure 9. The optimal allocation results is shown in Table 4, and the microgrid system costs is shown in Table 5.

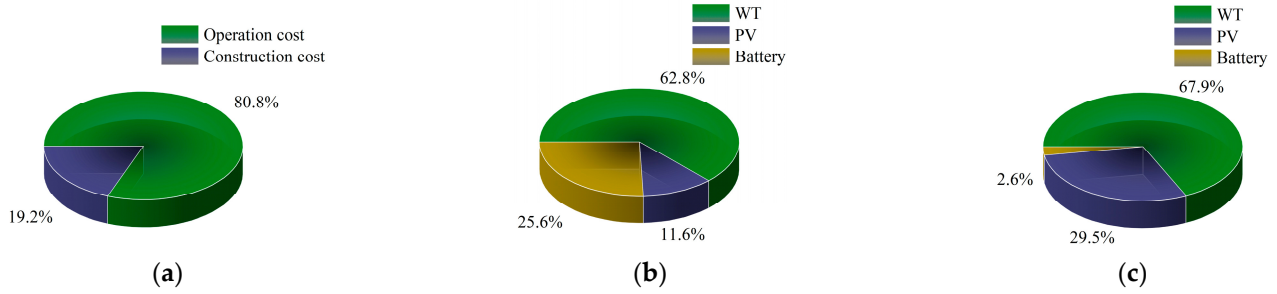


Figure 8. Cost structure. (**a**) Two-stage cost composition; (**b**) allocation cost composition; (**c**) power supply operation cost composition.

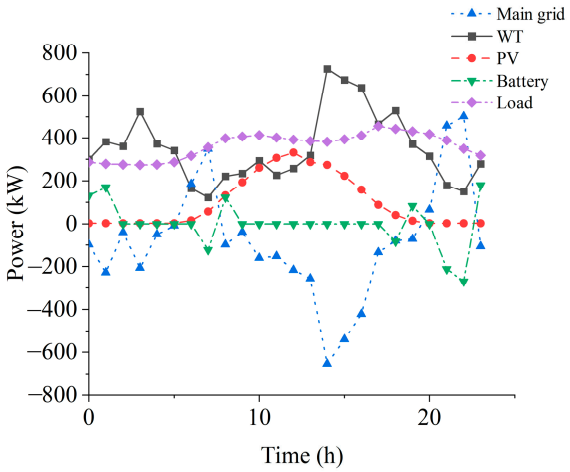


Figure 9. Typical daily scheduling.

Table 4. Optimal allocation results.

Wind Turbine Number	Photovoltaic Array Number	Battery Number	Total Cost (CNY)	Allocation Cost (CNY)	Operation Cost (CNY)
119	1220	173	4.36×10^7	8.16×10^6	3.54×10^7

Table 5. Microgrid system costs.

Cost \ Type	Wind Turbine	Photovolatic Array	Battery	Main Grid
Allocation cost (CNY)	5.12×10^6	9.43×10^5	2.09×10^6	
Operation cost (CNY)	2.71×10^7	1.18×10^7	1.03×10^6	-5.55×10^6

In the context of energy transformation, small microgrids should gradually reduce their dependence on the main grid to meet the load demand in the region, and small microgrids should also actively participate in grid connection to further promote energy transformation. Therefore, the allocation of energy storage equipment for microgrids is particularly important. The operation cost of the medium- and long-term planning of wind–solar–storage is the most important factor affecting the economy of the system. The introduction of a load demand response mechanism in the system is an effective means to reduce the operation cost. The influence of flexible load on the microgrid is analyzed in the next section of this paper.

5.3. Sensitivity Analysis of Flexible Load Adjustment Capability in Capacity Allocation

According to the rigid–flexible load ratios in the microgrid, ratios ranging from ten-to-zero to zero-to-ten correspond to A through K in that order. The corresponding load demand on a typical day is shown in Figure 10. It can be seen from Figure 11 that with the increase in the proportion of flexible load, the peaking and valley-filling effect of the load demand response model becomes more and more obvious. The period of high electricity price of the load shifts to a period of low electricity price, which relieves the pressure on the system to a certain extent. Based on this, Figure 11 illustrates the economic allocation and operation of the system under various rigid and flexible conditions.

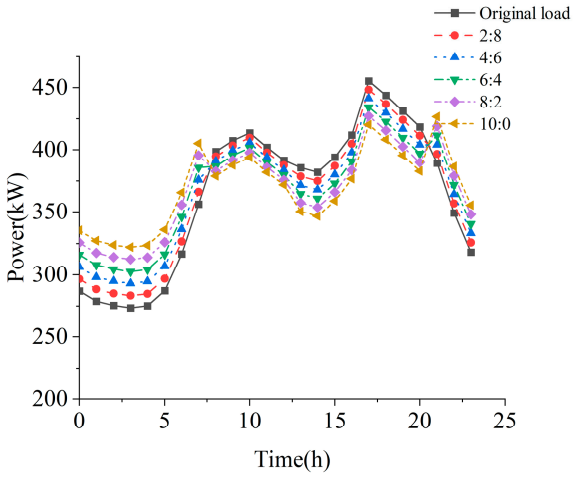


Figure 10. Load demand response of different rigid and flexible ratios.

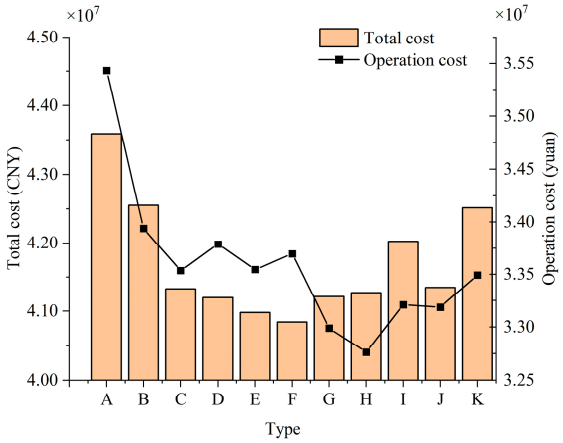


Figure 11. Economic allocation and operation of the system under different rigid and flexible ratios.

The optimization results are shown in Figure 11; when the rigid–flexible ratio reaches five-to-five, the total cost and construction cost of the microgrid reach the optimal level. At this time, the construction cost is CNY 7.14 million, and the operation cost is CNY 33.7 million. Compared with the rigid–flexible ratio of ten-to-zero, the allocation cost is reduced by CNY 1.01 million, and the operation cost is reduced by CNY 740,000. When the rigid–flexible ratio is three-to-seven, the operation cost of the system reaches the optimal level. The total cost is CNY 41.26 million. The operating cost accounts for CNY 32.76 million. Compared to a rigid–flexible ratio of ten-to-zero, the operating cost is reduced by CNY 1.67 million. The allocation cost of the system is mainly concentrated in the initial construction, and the operation cost is the long-term investment in the later period. Therefore, the next section of this paper analyzes the impact of planning years on the overall economic benefits of the wind and solar storage power generation system.

5.4. Sensitivity Analysis of Planning Years in Capacity Allocation

As shown in Figure 12, when the planning period is 5 years, the allocation cost and operation cost of the microgrid account for 46.12% and 53.88%, respectively, and the gap between the two is not large. When the planning period is 10 years, the operation cost of the microgrid is about twice the allocation cost; the operation cost is 66.90%, and the allocation cost is 33.10%. When the planning period is 20 years, the operation cost of the microgrid is much higher than its allocation cost, of which the operation cost accounts for 80.85% and the allocation cost accounts for 19.15%. From the perspective of average annual costs, the average annual total cost gradually decreases with the increase in planning years, but the average annual operation cost is not significantly affected by the planning years. The

reduction in the annual total cost is mainly due to the impact of planning years, improving the utilization rate of equipment, resulting in a reduction in the annual allocation cost.

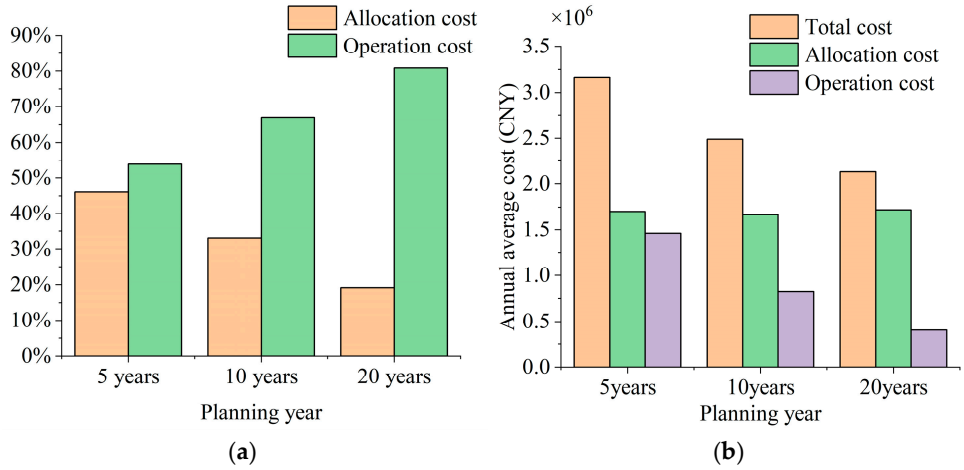


Figure 12. The influence of different planning years on capacity planning. (**a**) Two-stage costs under different planning years; (**b**) average annual costs for different planning years.

In general, the longer the planning years, the higher the overall economic benefits of the microgrid. However, as the number of planning years increases, the economic benefits gradually diminish. When the number of planning years exceeds 20, the power generation equipment of the microgrid will generally reach the end of its service life. At that time, the failure rate of the entire system will increase rapidly. The fluctuations in the power of the grid will gradually become higher. It cannot meet the fluctuation requirements of the power of the grid, resulting in significant underutilization of solar and wind power.

5.5. Algorithm Comparison

To verify the accuracy and superiority of ISOA, this paper compares Particle Swarm Optimization (PSO) with unimproved SOA in a small microgrid in southern China to solve a scenario with a planning life of 20 years and a rigid–flexible load ratio of five-to-five. The cost of capacity allocation of the microgrid and the convergence of the algorithm are shown in Table 6. In the case of the same number of iterations, the improved snake optimization algorithm has the lowest cost and the smallest number of iterations reaching convergence. The iterative process of the three algorithms is shown in Figure 13. Table 6 shows that the computation time of ISOA is significantly longer than that of SOA, but shorter than POS. The computation times for POS, ISOA and SOA are 14,051.99 s, 9412.30 and 2519.73 s, respectively. The computational load of ISOA is approximately 3.7 times that of SOA, which leads to the longer computation time for ISOA. However, ISOA significantly enhances the global optimization capability, achieving the lowest number of convergence iterations and the optimal solution.

Table 6. Algorithm comparison result.

Algorithm	Total Cost (Thousand CNY)	Total Population	Iterations	Convergence Iterations	Computation Time/s
ISOA	40,408	300	500	42	9412.30
SOA	40,986	300	500	151	2519.73
POS	41,335	300	500	185	14,051.99

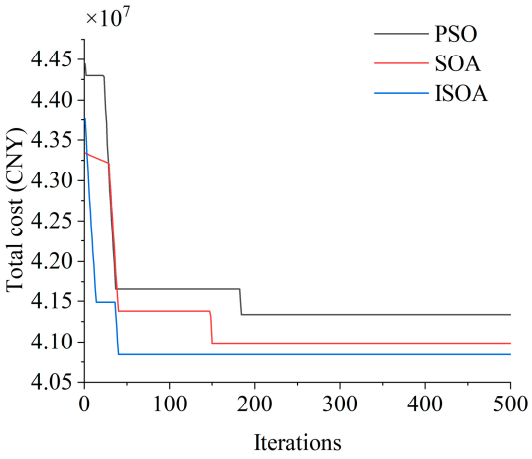


Figure 13. Algorithm iteration graph.

Table 7 shows the optimal allocation and cost composition for each algorithm. ISOA yields the smallest battery capacity, followed by SOA, with POS requiring the largest. Additionally, ISOA achieves the largest wind turbine capacity and the smallest photovoltaic array capacity, while SOA achieves a wind turbine capacity slightly smaller than POS and a photovoltaic array capacity greater than POS. Cost analysis shows that ISOA achieves the best optimization results, with SOA close behind and significantly better than POS. These results indicate that the most critical factor affecting the economy of capacity allocation is the battery. As an energy storage device, the battery does not generate direct economic benefits. Therefore, minimizing battery capacity while ensuring safe and stable system operation enhances system economy. In terms of convergence speed, ISOA is the fastest, followed by SOA and then POS. The results demonstrate that the ISOA exhibits strong optimization capability and fast convergence.

Table 7. Cost structure analysis.

Algorithm	ISOA	SOA	POS
Wind turbine number	129	110	119
Photovoltaic array number	697	1644	1389
Battery number	87	118	173
Total cost (thousand CNY)	40,408	40,986	41,335
Allocation cost (thousand CNY)	7143	7432	8158
Operation cost (thousand CNY)	33,697	33,553	33,177

6. Conclusions

This paper aims to optimize the capacity of grid-connected microgrids through a double-layer optimization model in order to improve the consumption rate of new energy and reduce carbon emissions. The upper layer consists of a capacity allocation model, where the capacities of wind turbines, photovoltaic arrays and batteries are the decision variables. The lower layer features an optimal scheduling model, with the outputs of each power source in the microgrid as the decision variables. Additionally, this paper examines capacity optimization for wind–solar–storage systems across various scenarios, exploring optimal capacity configurations and operational strategies. The paper concludes with the following findings:

(1) The two-layer optimization model presented herein effectively addresses the coupling issue between capacity and scheduling optimization. The results show that the allocation stage accounts for 19.2% of total costs, with wind turbines contribut-

ing 62.8% of these costs. In the operation stage, which makes up 80.8% of the total, wind turbines account for 67.9% of costs. It not only ensures a cost-effective capacity allocation but also considers economic factors in subsequent operational stages. The model also demonstrates that whole life cycle planning of wind–solar–storage systems can improve economic performance, particularly by focusing on reducing operational costs.

(2) The demand response model based on the TOU tariff is effectively characterized. At a rigid–flexible ratio of five-to-five, the total cost reaches its optimal level. A three-to-seven ratio achieves the lowest operational costs. The results indicate that an optimal ratio of rigid–flexible load can significantly improve economic efficiency. Meanwhile, the total cost and operation cost of the wind–solar–storage system in whole life cycle planning are not entirely consistent.

(3) The number of planning years significantly influences the microgrid's subsequent operating costs. Longer planning years result in higher operating costs, which account for a larger proportion of the total costs. Meanwhile, the higher the number of planning years, the lower the average annual cost of the microgrid. Comparative analysis of various planning horizons reveals that longer planning periods can improve economic efficiency of wind–solar–storage systems. Consequently, future landscape storage capacity planning should adopt a multi-temporal perspective.

(4) The ISOA is proposed to tackle the complexities of a nonlinear and multivariable two-layer model. Comparative analysis demonstrates that the ISOA notably enhances global optimization search capability and robustness in contrast to the conventional SOA and POS algorithms. This approach offers significant advantages in addressing challenges like the two-layer optimization model for capacity allocation in wind–solar–storage systems.

This study demonstrates that optimizing the capacity of wind–solar–storage systems based on a two-layer optimization model effectively resolves the intricate coupling between capacity and scheduling optimization. The proposed model solution is applicable for comprehensive life cycle planning of wind–solar–storage systems and provides valuable guidance for the construction and grid integration of various new energy power plants. Future research could extend the application of this model to other types of new energy power generation systems, thereby facilitating the systematic and orderly advancement of energy transformation efforts. Meanwhile, this article attempts to establish ISOA to solve the two-layer model for microgrid capacity optimization. To improve the global search capability of the algorithm, other optimization algorithms are introduced, for which increases in complexity led to a higher computational load. As a result, the computation time for ISOA became longer, presenting certain limitations. Balancing the enhancement of the algorithm's global search ability with a reasonable computational load will be a meaningful direction for future research.

Author Contributions: M.Z.: writing—original draft. Y.H.: writing—review and editing. Y.T.: writing—review and editing. K.S.: methodology. L.J.: conceptualization, data curation. H.W.: validation. All authors have read and agreed to the published version of the manuscript.

Funding: This research was funded by the Science and Technology Project of China Southern Power Grid Co., Ltd. (GDKJXM20230402).

Data Availability Statement: The original contributions presented in the study are included in the article; further inquiries can be directed to the corresponding authors.

Conflicts of Interest: M.Z. is employed by the company Power Grid Planning Research Center of Guangdong Power Grid Co., Ltd. The remaining authors declare that the research was conducted in the absence of any commercial or financial relationships. The authors declare no conflicts of interest.

References

1. Wei, Y.M.; Chen, K.; Kang, J.N.; Chen, W.; Wang, X.Y.; Zhang, X. Policy and management of carbon peaking and carbon neutrality: A literature review. *Engineering* **2022**, *14*, 52–63. [CrossRef]
2. Impram, S.; Nese, S.V.; Oral, B. Challenges of renewable energy penetration on power system flexibility: A survey. *Energy Strategy Rev.* **2020**, *31*, 100539. [CrossRef]
3. Fu, H.; Wang, J.; Cui, Y.; Si, Y.; Xia, D.; Ma, X. Capacity optimization configuration of live gas storage system in independent power systems. *Int. J. Thermofluids* **2024**, *21*, 100526. [CrossRef]
4. Modu, B.; Abdullah, M.P.; Bukar, A.L.; Hamza, M.F.; Adewolu, M.S. Operational strategy and capacity optimization of standalone solar-wind-biomass-fuel cell energy system using hybrid LF-SSA algorithms. *Int. J. Hydrogen Energy* **2024**, *50*, 92–106. [CrossRef]
5. Yang, A.; Wang, H.; Li, B.; Tan, Z. Capacity optimization of hybrid energy storage system for microgrid based on electric vehicles' orderly charging/discharging strategy. *J. Clean. Prod.* **2023**, *411*, 137346. [CrossRef]
6. Hemmati, M.; Bayati, N.; Ebel, T. Life Cycle Assessment and Costing of Large-Scale Battery Energy Storage Integration in Lombok's Power Grid. *Batteries* **2024**, *10*, 295. [CrossRef]
7. Wang, C.; Jiao, S.; Li, Y.; Zhang, Q. Capacity optimization of a hybrid energy storage system considering wind-Solar reliability evaluation based on a novel multi-strategy snake optimization algorithm. *Expert Syst. Appl.* **2023**, *231*, 120602. [CrossRef]
8. Mu, C.; Shi, Y.; Xu, N.; Wang, X.; Tang, Z.; Jia, H.; Geng, H. Multi-Objective Interval Optimization Dispatch of Microgrid via Deep Reinforcement Learning. *IEEE Trans. Smart Grid* **2024**, *15*, 2957–2970. [CrossRef]
9. Chen, W.; Wang, Z.; Hu, J.; Han, Q.-L.; Liu, G.-P. Privacy-Preserving Distributed Economic Dispatch of Microgrids Using Edge-Based Additive Perturbations: An Accelerated Consensus Algorithm. *IEEE Trans. Syst. Man Cybern. Syst.* **2024**, *54*, 2638–2650. [CrossRef]
10. Hemmati, M.; Bayati, N.; Ebel, T. Integrated Optimal Energy Management of Multi-Microgrid Network Considering Energy Performance Index: Global Chance-Constrained Programming Framework. *Energies* **2024**, *17*, 4367. [CrossRef]
11. Hemmati, M.; Mohammadi-Ivatloo, B.; Ghasemzadeh, S. Risk-based optimal scheduling of reconfigurable smart renewable energy based microgrids. *Int. J. Electr. Power Energy Syst.* **2018**, *101*, 415–428. [CrossRef]
12. Chen, W.; Wang, Z.; Ge, Q.; Dong, H.; Liu, G.-P. Quantized Distributed Economic Dispatch for Microgrids: Paillier Encryption–Decryption Scheme. *IEEE Trans. Ind. Inform.* **2024**, *20*, 6552–6562. [CrossRef]
13. Yan, M.; Peng, S.E.; Lai, C.S.; Chen, S.-Z.; Liu, J.; Xu, J.; Xu, F.; Lai, L.L.; Chen, G. Two-Layer Optimization Planning Model for Integrated Energy Systems in Hydrogen Refueling Original Station. *Sustainability* **2023**, *15*, 7941. [CrossRef]
14. Hemmati, M.; Abapour, M.; Mohammadi-Ivatloo, B.; Anvari-Moghaddam, A. Optimal Operation of Integrated Electrical and Natural Gas Networks with a Focus on Distributed Energy Hub Systems. *Sustainability* **2020**, *12*, 8320. [CrossRef]
15. Wang, Z.; Zhang, Z.; Zhang, Z.; Lei, D.; Li, M.; Zhang, L. Two-layer optimization of integrated energy system with considering ambient temperature effect and variable operation scheme. *Energy* **2023**, *278*, 127671. [CrossRef]
16. Ji, X.; Li, C.; Li, D.; Qi, C. Bidding strategy of two-layer optimization model for electricity market considering renewable energy based on deep reinforcement learning. *Electronics* **2022**, *11*, 3107. [CrossRef]
17. Phommixay, S.; Doumbia, M.L.; Cui, Q. A two-stage two-layer optimization approach for economic operation of a microgrid under a planned outage. *Sustain. Cities Soc.* **2021**, *66*, 102675. [CrossRef]
18. Abdalla, A.N.; Nazir, M.S.; Tao, H.; Cao, S.; Ji, R.; Jiang, M.; Yao, L. Integration of energy storage system and renewable energy sources based on artificial intelligence: An overview. *J. Energy Storage* **2021**, *40*, 102811. [CrossRef]
19. Shewale, A.; Mokhade, A.; Funde, N.; Bokde, N.D. An overview of demand response in smart grid and optimization techniques for efficient residential appliance scheduling problem. *Energies* **2020**, *13*, 4266. [CrossRef]
20. Javed, M.S.; Ma, T.; Jurasz, J.; Amin, M.Y. Solar and wind power generator systems with pumped hydro storage: Review and future perspectives. *Renew. Energy* **2020**, *148*, 176–192. [CrossRef]
21. He, Y.L.; Wu, X.W.; Sun, K.; Du, X.; Wang, H.; Zhao, J. Economic Optimization Scheduling Based on Load Demand in Microgrids Considering Source Network Load Storage. *Electronics* **2023**, *12*, 2721. [CrossRef]
22. Zhao, J.L.; Zeng, S.M.; Xu, W.T.; Du, X.D.; He, Y.L. Optimized self-adaptive power distribution for microgrids in a typical tourism water village of northern china under COVID-19 background. *Sustainability* **2022**, *14*, 9839. [CrossRef]
23. Wang, H.; Wu, X.; Sun, K.; He, Y. Research on the optimal economic power dispatching of a multi-microgrid cooperative operation. *Energies* **2022**, *15*, 8194. [CrossRef]
24. Wen, L.; Zhou, K.; Feng, W.; Yang, S. Demand side management in smart grid: A dynamic-price-based demand response model. *IEEE Trans. Eng. Manag.* **2022**, *71*, 1439–1451. [CrossRef]
25. Hemmati, M.; Mohammadi-Ivatloo, B.; Anvari-Moghaddam, A. Optimal chance-constrained scheduling of reconfigurable microgrids considering islanding operation constraints. *IEEE Syst. J.* **2020**, *14*, 5340–5349. [CrossRef]
26. Hashim, F.A.; Hussien, A.G. Snake Optimizer: A novel meta-heuristic optimization algorithm. *Knowl.-Based Syst.* **2022**, *242*, 108320. [CrossRef]
27. Varol Altay, E.; Alatas, B. Bird swarm algorithms with chaotic mapping. *Artif. Intell. Rev.* **2020**, *53*, 1373–1414. [CrossRef]
28. Yu, Y.; Gao, S.; Cheng, S.; Wang, Y.; Song, S.; Yuan, F. CBSO: A memetic brain storm optimization with chaotic local search. *Memetic Comput.* **2018**, *10*, 353–367. [CrossRef]

29. Yang, X.S.; Suash, D. Cuckoo search via Lévy flights. In Proceedings of the 2009 World Congress on Nature & Biologically Inspired Computing (NaBIC), Coimbatore, India, 9–11 December 2009; pp. 210–214.
30. Høibakk, R.; Lukkassen, D.; Meidell, A.; Persson, L.-E. Geometric Construction of Some Lehmer Means. *Mathematics* **2018**, *6*, 251. [CrossRef]

Disclaimer/Publisher's Note: The statements, opinions and data contained in all publications are solely those of the individual author(s) and contributor(s) and not of MDPI and/or the editor(s). MDPI and/or the editor(s) disclaim responsibility for any injury to people or property resulting from any ideas, methods, instructions or products referred to in the content.